Direct measurement of near surface seismic body wave dispersion from uncorrelated vibroseis data

Kris Innanen

ABSTRACT

The propensity of geological volumes, particularly in the near surface, to cause seismic body waves to propagate dispersively is a serious impediment to FWI. Anelastic parameters, like Q_P and Q_S, can appear as unknowns in tractable seismic inverse algorithms, provided the associated dispersion laws are known. However, general attenuation factors with arbitrary variability in space and frequency cannot be solved for. If a FWI scheme solves for elastic and anelastic properties given an accurate prior knowledge of the dispersion law, we will require a flexible and unconstrained procedure for determining this law; one which occurs relatively early in the processing flow. An example of such a procedure is illustrated in this paper, based on picking arrival times from the Gabor spectra of uncorrelated vibe sweeps measured in a walkaway VSP experiment. Estimating phase velocity as the ratio of the source/receiver ray path length to the departure/arrival time difference of each frequency in the sweep, a remarkably consistent set of $V_P(f)$ estimates are derived for 20 depth levels between 76m and 116m depth. Calibrating these to match group velocities measure with standard time domain slopes, a range between roughly 500m/s and 2000m/s, from 10Hz to 70Hz is calculated. The curves are sigmoidal, with a negative curvature that does not match with standard logarithmic models.

INTRODUCTION

In a recent Society of Exploration Geophysicists annual meeting workshop (W-12: The limit of FWI in subsurface parameter recovery; Fri Oct 23 2015, New Orleans LA USA), the issue of the anelasticity of the subsurface — in the near surface particularly — was several times pointed to as an obstacle to the recovery of elastic medium properties using full waveform inversion (FWI) methods. In particular, in the panel discussion, a common misconception was discredited, which is that because FWI focuses on low frequencies, intrinsic absorption is a relatively unimportant mechanism. While it is true that at low frequencies *attenuation* is relatively weak, the influence of the accompanying body wave *dispersion* (Aki and Richards, 2002; Kjartansson, 1979; Futterman, 1962) increases at low frequencies, and neglect of this phenomenon is potentially devastating to velocity model building and more ambitious multiparameter FWI.

An FWI processing flow which accounts for anelasticity could take on several alternative forms, analogous to the those selected in depth migration in the presence of Q. One possibility is to include attenuation and dispersion parameters as elements of the suite of unknowns to be simultaneously determined in a single FWI loop. This has been considered by a range of researchers in the context of FWI proper (Ribodetti and Virieux, 1998; Hicks and Pratt, 2001; Hak and Mulder, 2010a,b; Kamei and Pratt, 2013; Métivier et al., 2015), and in the context of scattering, both for the derivation of FWI sensitivities (Moradi and Innanen, 2015) and for direct inversion (Innanen and Weglein, 2007; Innanen and Lira, 2010). Another possibility is to formulate full elastic FWI schemes, having first done the

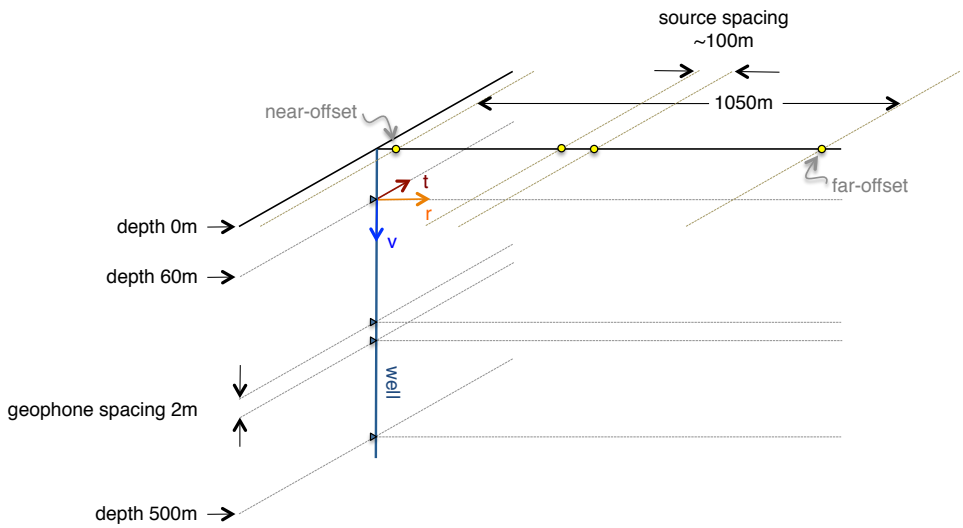

FIG. 1. Geometry and scale of the VSP experiment.

sensitive preprocessing necessary to estimate (e.g., Tonn, 1991; Zhang and Ulrych, 2007; Margrave, 2015) and remove (e.g., Hargreaves and Calvert, 1991) the effects of anelasticity. Without the introduction of some new ideas, however, both of these alternatives rely on the *a priori* selection of an absorptive model type. This selection is in current practice ad hoc, with choices guided more by ease of use rather than geophysical aptness. The point of view taken in this paper is that in a FWI scheme, with its sensitive dependence on the detailed information in a waveform, ad hoc selection will probably not suffice.

To exemplify the problem, consider a common model for attenuation and dispersion taken from Aki and Richards (2002). The acoustic/elastic phase velocity c is replaced by

$$V_P(\mathbf{r},\omega) = V_{P_0}(\mathbf{r})\left[1 - \frac{i}{2Q(\mathbf{r})} + \frac{1}{\pi Q(\mathbf{r})}\log\left(\frac{\omega}{\omega_0(\mathbf{r})}\right)\right], \tag{1}$$

where ω is the angular frequency, ω_0 is a reference frequency, V_{P_0} is the phase velocity at the reference frequency, and Q is the quality factor. This is a powerful and practical model: amongst other features, it corresponds with a legitimate Kramers-Krönig pair over the seismic bandwidth, producing a causal waveform, while introducing only two new parameters, $Q(\mathbf{r})$ and $\omega_0(\mathbf{r})$, to be constrained by seismic observations. The latter aspect is critical: arbitrary variations of a complex wave velocity in both space and frequency, i.e.,

$$V_P(\mathbf{r},\omega) = V_{P_R}(\mathbf{r},\omega) + iV_{P_I}(\mathbf{r},\omega), \tag{2}$$

cannot be constrained with surface seismic data (Innanen and Weglein, 2007). In contrast, in equation (1) the spatial variations of the properties are unknown, but the frequency dependence of the model is provided a priori - with this prior information, seismic data can constrain the remaining unknowns. The cost of this is that we must decide in advance that the phase velocity obeys the rule in equation (1), which, though physically reasonable, constitutes a free floating assumption.

A future in which through waveform fitting we are able to simultaneously determine anelastic and elastic properties, *if and only if* we have first selected a meaningful body wave dispersion model, seems plausible. The position we take in this paper is that robust, and simple, methods for such selection, will be an important technological requirement. Furthermore, such a method would have to be applicable early on in a workflow, before processing which implicitly assumes one or other physical model has been carried out, and it would have to analyze dispersive behaviour in an unconstrained manner, i.e., without assuming a certain dispersion model was in place.

The purpose of this paper is to report on a methodology with many of these positive features. The approach is based on the sensitivity of uncorrelated vibroseis data to the frequency dependence of seismic velocities. This sensitivity was first discussed in a marine setting, in which the motion of the vibrating source was seen to give rise to an apparent dispersive, or Doppler, effect, which had to be corrected for (Dragoset, 1988). Sun and Milkereit (2007) and Sun et al. (2009) proposed that this sensitivity be used to characterize proper body wave dispersion, and applied it in a correlation scheme on VSP data to characterize dispersion in the vicinity of the Mallik gas hydrate research well. Subsequently Haase (2010) applied the approach to modelled VSP data from velocity and density logs. Here we assemble a processing regimen based on these same ideas, organized to focus on body wave dispersion in the near surface. We make use of a well-characterized multicomponent walkaway VSP data set wherein we can focus on ray paths confined to the upper 150m, where dispersion and attenuation are both very strong and poorly characterized. The field results, which are based on sufficient trials to define a mean phase velocity curve and +/- one standard deviation bounds, are indicative of very significant dispersion in the low frequencies.

DATA SET

A walkaway vertical seismic profiling (VSP) data set was acquired in Western Canada in 2011 (Hall et al., 2012). Dynamite and vibroseis sources were shot into 3C sensors; in this study we will consider only the vibroseis source shot into the vertical components of the sensors. The source was an EnviroVibe using a linear sweep of 10-300Hz over 20s, with near offset shot point 12m from the borehole and far offset shot point 1031m from the borehole. The subset of the data used in this study correspond to the responses of geophones at 20 depth levels, between 76-116m, to the source at 320m offset from the borehole. In Figure 1 source and sensor depths and intervals are further detailed.

The ray paths we consider are therefore restricted to the upper region of the geological volume. An independent study of shallow Q_P and Q_S on the same data set (Montano et al., 2015) found a stable and relatively constant value of $Q_P = 20$ in the upper 150m, supporting our current assumption of homogeneous dispersive properties, and also suggesting that the region has a sufficiently low Q to produce significant dispersion.

The near offset shot record from the walkaway experiment is illustrated in Figure 2, with the direct arrival in the upper 150m picked and illustrated with a red solid line. The velocity is estimated at 1940m/s. Because the pick was made by identifying the first breaks, this velocity estimate reflects the rate at which the higher frequency components of the

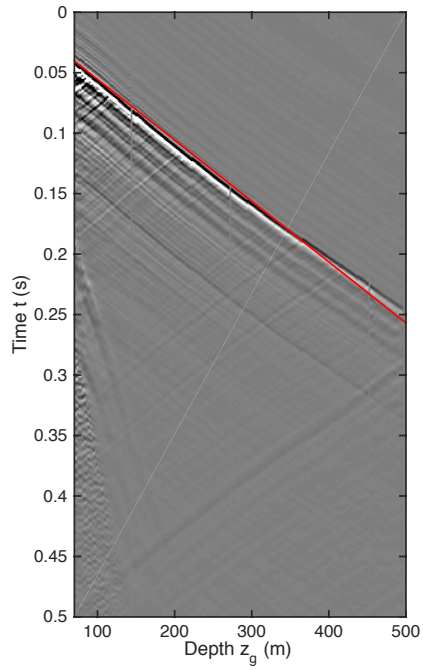

FIG. 2. Near offset shot record, with direct arrival in the upper 150m picked and illustrated with a solid red line.

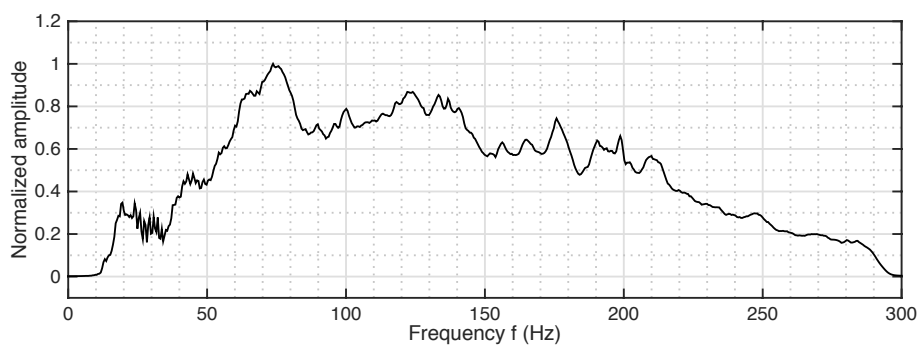

FIG. 3. Average amplitude spectrum of the zero offset traces illustrated in Figure 2.

wave propagate. This value will be used to calibrate the phase velocity estimate later in the development. In Figure 3 the average amplitude spectrum of the traces in Figure 2 is plotted. The dominant frequency is 74Hz.

METHODOLOGY

The phase velocity is calculated by determining the ratio of the propagation distance of the direct P-wave arrival to the traveltime associated with a particular frequency f. The propagation distance is determined from the locations of the source and receiver in question and the assumption of straight ray paths. The travel time is the difference between the time at which frequency f arrives at the sensor and the time the same frequency departs from the source. These latter data are determined from time-frequency analysis of the uncorrelated vibroseis traces.

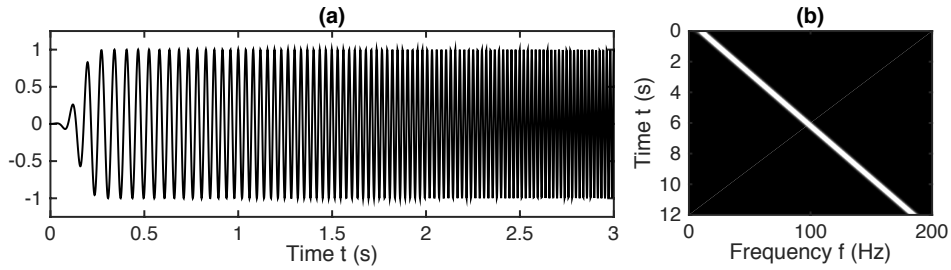

FIG. 4. The programmed sweep used in the VSP survey. (a) The first 3.0s of the sweep in the time domain, with cosine taper at early times. (b) The first 12.0s of the sweep in the time-frequency domain via the Gabor transform.

Time of departure of frequency f from source

In Figure 4a the first 3s of the programmed sweep used in the VSP experiment is illustrated; in Figure 4b the Gabor transform of the sweep over the first 12s is illustrated. The transform was calculated using the function *fgabor.m* in the CREWES Matlab Library (see *www.crewes.org*). The sweep is modelled mathematically as $s(t)$:

$$s(t) = \text{Im}\left[a(t)e^{i\phi(t)}\right], \tag{3}$$

with the role of the amplitude $a(t)$ being primarily to taper early and late times, and the phase having the time dependence of the frequency, $f(t)$, encoded in it:

$$\phi(t) = 2\pi f(t)t. \tag{4}$$

A linear sweep has the form

$$f(t) = f_{\text{min}} + \left(\frac{f_{\text{max}} - f_{\text{min}}}{T}\right)t, \tag{5}$$

parameterized by the low frequency limit f_{min}, the high frequency limit f_{min}, and the sweep length T. The inverse of the function $f(t)$ is the time at which frequency f departs into the Earth from the vibe pad. Calling this time $\tau_S(f)$, we have that frequency f departs along its wave path at time

$$\tau_S(f) = t(f) = \left(\frac{f - f_{\text{min}}}{f_{\text{max}} - f_{\text{min}}}\right)T, \tag{6}$$

relative to the sweep start time $t = 0$.

Time of arrival of frequency f at geophone

The geophones in the borehole detect the raw sweep after it has propagated through the near surface (Figure 5). Assuming a straight ray path, a surface offset of the source to the borehole of x_s and a depth to the geophone of z_g, the time $\Delta\tau(f)$ it takes for the seismic wave at frequency f to propagate to the geophone satisfies

$$\Delta\tau^2(f) = \frac{x_s^2 + z_g^2}{V_P^2(f)}, \tag{7}$$

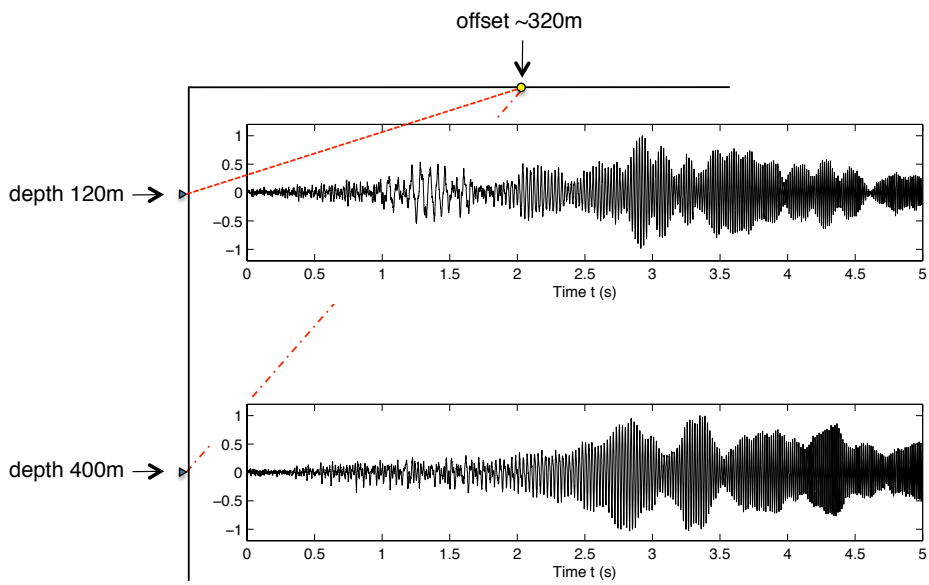

FIG. 5. Uncorrelated signals arriving from a source offset 320m from the borehole at geophones at depths of 120m and 400m deep.

where $c(f)$ is the P-wave phase velocity. Then, the time $\tau_M(f)$ at which the frequency f arrives at a particular depth z_g after propagating a distance $L = (x_s^2 + z_g^2)^{1/2}$ through the Earth volume is, from equations (6)-(7), given by

$$\tau_M(f) = \tau_S(f) + \frac{L}{V_P(f)}. \tag{8}$$

Phase velocity calculation and calibration

As discussed above, the geometry of the source and receiver and the assumption of a straight ray path provides L. The Gabor transform of the programmed sweep (i.e., Figure 4b), and/or the formula in equation (6) given sweep parameters, as desired, provides the time of departure $\tau_S(f)$ of each frequency. Finally, the Gabor transform of the measured sweep at the geophone provides the time of arrival $\tau_M(f)$ of each frequency. With these quantities in hand, equation (8) can be used to find the average dispersive wave velocity experienced by the wave:

$$V_{P_{\text{raw}}}(f) = \frac{L}{\tau_M(f) - \tau_S(f)}. \tag{9}$$

We refer to this as the raw, or uncalibrated phase velocity. The τ_M and τ_S picks can be done with high relative accuracy, but are exposed to an overall constant error. To account for this we introduce a calibration time τ_{cal}, constant for the whole suite of traces analyzed, to be determined using independent data. The final estimate is then the calibrated phase velocity $V_{P_{\text{cal}}}(f)$:

$$V_{P_{\text{cal}}}(f) = \frac{L}{\tau_M(f) - \tau_S(f) - \tau_{\text{cal}}}. \tag{10}$$

The choice of τ_{cal} and its justification are discussed in the following section.

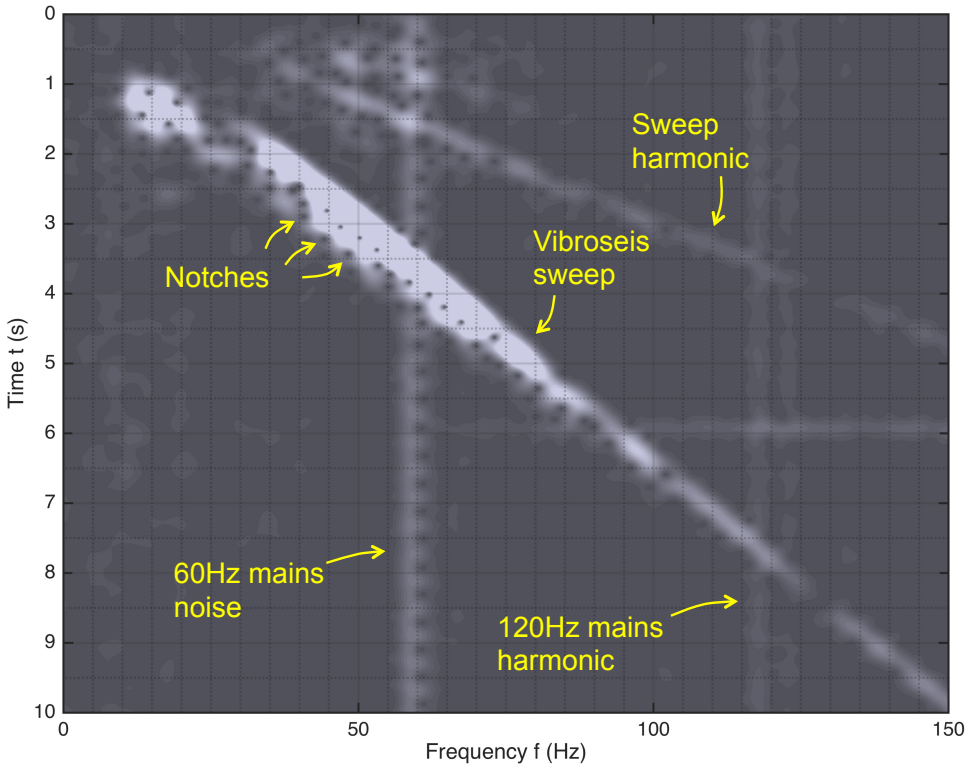

FIG. 6. Gabor spectrum of a single uncorrelated trace (depth $z_g = 76$m, offset $x_s = 320$m). Notches, mains noise and harmonics, and sweep and harmonic are labelled. Event labelled "vibroseis sweep" is analyzed in this study.

RESULTS

The main effort in applying equation (10) to field data is in calculating τ_M from the geophone responses (examples of which are plotted in Figure 5). The Gabor transform of an example uncorrelated trace is illustrated in Figure 6, with its main features labelled. The event labelled "vibroseis sweep" contains the information of current interest.

Our interest is in the time at which a particular frequency component of the wave first arrives at the geophone. This requires the "top" of the vibroseis sweep to be picked. Already by eye the effect of body wave dispersion is visible: the sweep program is linear, but the arrival times of the lower frequencies in Figure 6 describe a curve tending more horizontal as $f \to 0$. At higher frequencies the rate of arrival of frequencies becomes constant.

A semi-automatic picking procedure was used. On the assumption of smooth deviations of the measured traveltime vs frequency away from linear, a low (4th) order polynomial was fit to each Gabor spectrum based on between 10 and 15 picks of the first arrival of energy. What constitutes the precise first arrival is arbitrary, but provided a consistent choice is made, any systematic error can be corrected with the calibration term in equation (10). Normalizing all Gabor spectra and analyzing images with a fixed clip level appears to

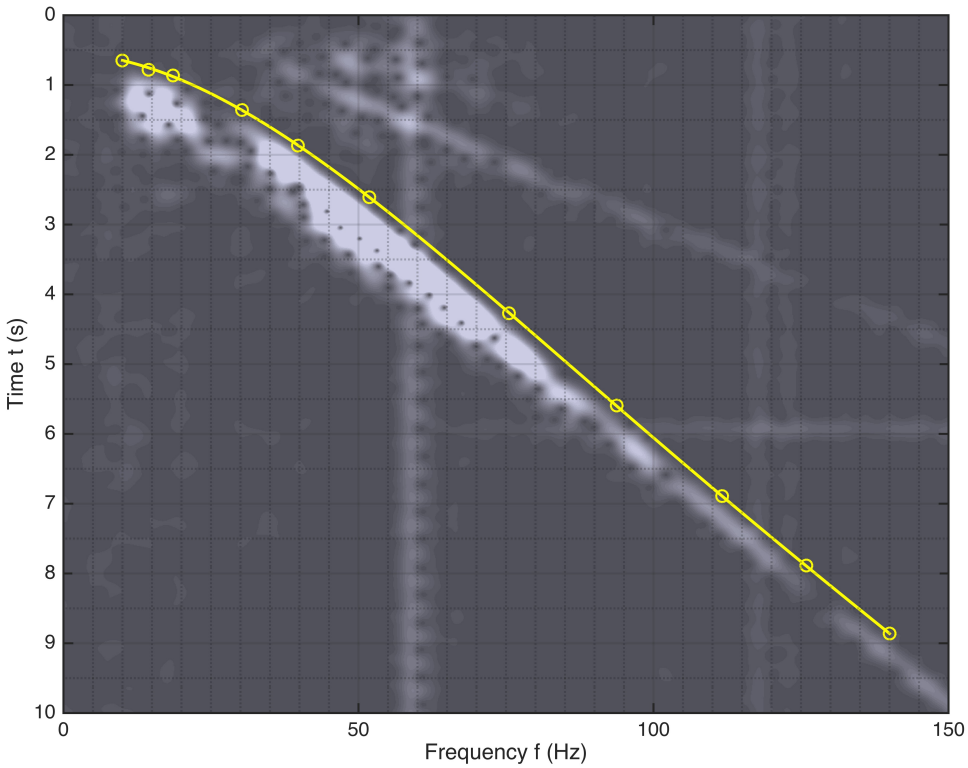

FIG. 7. Example of arrival time picking procedure. A smooth variation of arrival time with frequency is assumed, such that 10-15 picks can be fit with a low (4rth) order polynomial.

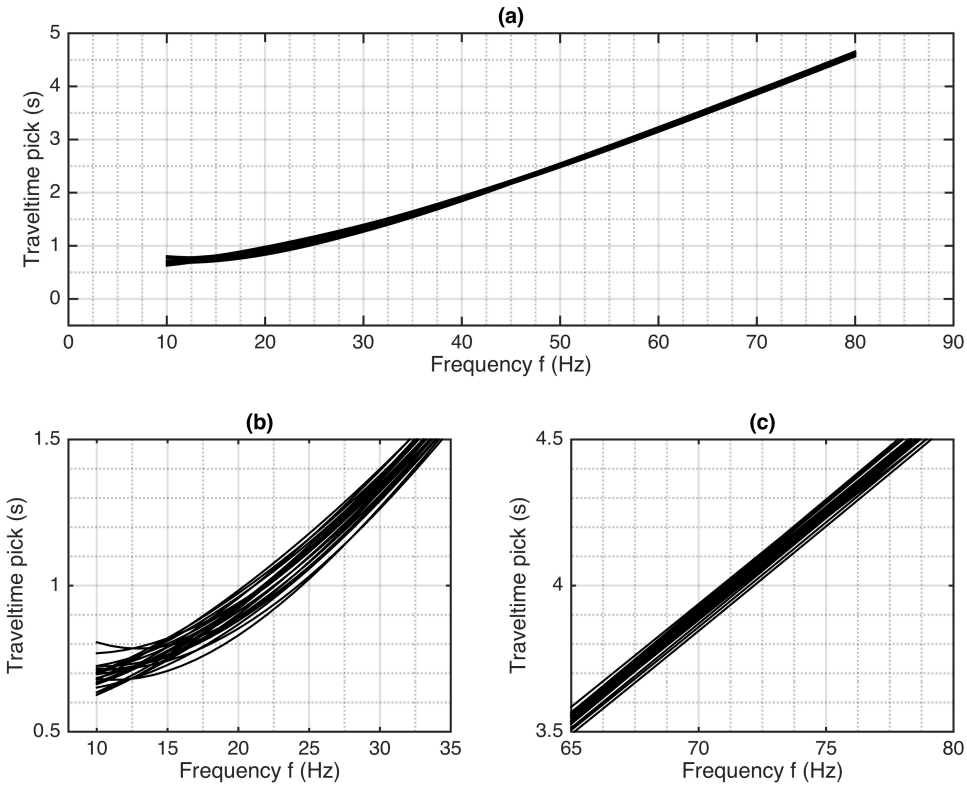

FIG. 8. Summary of 20 travel time vs. frequency curves. (a) Full picks between 10Hz and 80Hz. Note the departure from linear at low frequencies. (b)-(c) Details at low and high frequency ranges.

provide a workable environment for consistent picking; an example set of picks and fitted curve are illustrated in Figure 7.

This procedure was carried out on 20 traces, the responses of geophones between depths of 76m and 116m to the source at 320m offset. The results are summarized in Figure 8. In Figure 8a the full results are plotted. The leading order variation, which is the departure of the arrival time vs frequency curve from linear at low frequencies, is visible. To illustrate some of the variability in the results, in Figures 8b-c we zoom in to low (b) and high (c) frequencies.

The results illustrated in Figure 8 are the τ_M values needed to compute $V_{P_{\text{raw}}}(f)$ from equation (10). Although available directly from the sweep program parameters and equation (6), in the results the τ_S values were picked from a Gabor spectrum of the programmed sweep. This forces the departure time τ_S values to be determined with the same bias as that with which the arrival times τ_M are determined, decreasing the influence of either on the difference in equation (10).

The raw phase velocities are then calculated for each trace. These are illustrated in Figure 9. In Figure 9a the individual calculated phase velocity curves are illustrated, and in Figure 9b the mean curve is illustrated, bounded on either side by a single standard deviation. Let us make two criticisms of this uncalibrated result. First, in the plot the

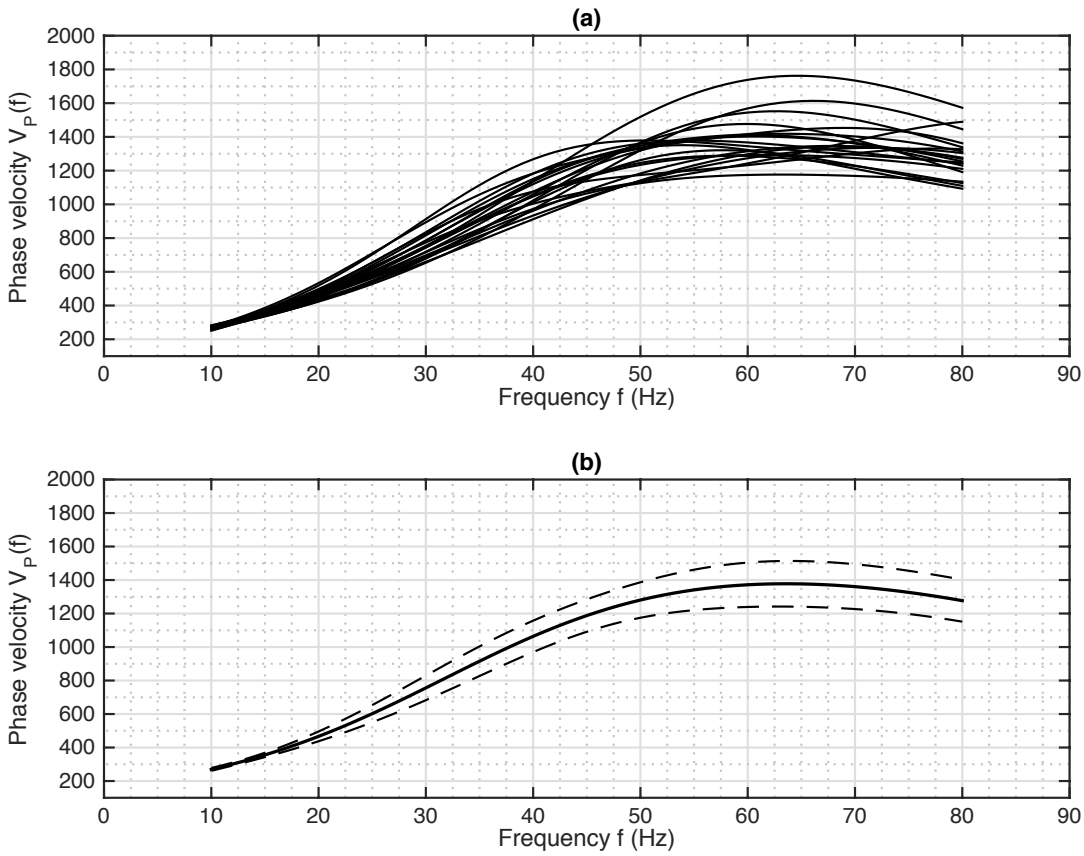

FIG. 9. Raw phase velocity estimation results: (a) for each of twenty geophone responses; (b) the mean (solid line) and $\pm$ one standard deviation (dashed line).

curves between 75-80Hz exhibit increasingly high amplitude oscillations, in spte of the fact that in the picked arrival times they appear to settle out at high frequency. This is because small oscillations in the fitted polynomial are magnified in the velocity calculation wherein they appear in the denominator. Going forward we will consider the results as being properly constrained only up to roughly 70Hz. Visual examination of the Gabor spectrum, and experience from analytic models of body wave dispersion, both lead to the expectation that the phase velocity curve will approach a fixed maximum value matching that which standard time-domain velocity analysis produces. Thus, curve fitting component of the procedure restricts our range of trustworthy $V_{P_{\text{raw}}}(f)$ values to between 10-70Hz, i.e., up to the dominant frequency of the experiment.

The second criticism concerns the value of the phase velocity being approached by the mean of the $V_{P_{\text{raw}}}(f)$ curves in the higher frequency range, which is roughly 1400m/s. This is significantly lower than the 1940m/s determined for the group propagating in the same depth interval, as illustrated in Figure 2. Since the high frequency maximum of $V_{P_{\text{raw}}}(f)$ is the rate at which the leading edge of the waveform propagates, these two numbers should be a much closer match.

The discrepancy is best explained as the result of residual bias between the arrival times τ_M and the programmed departure times τ_S picked from the Gabor spectra. Thus, it is best corrected for using the calibration quantity τ_{cal}. We now select τ_{cal} to be the quantity which brings the mean $V_{P_{\text{cal}}}(f)$ curve up to match 1940m/s at the dominant frequency of 74Hz. Thus, the two analysis procedures carried out in the earlier section are used to guide the calibration of the final $V_{P_{\text{cal}}}(f)$ curves. The calibration is carried out on each individual trace, with results as illustrated in Figure 10; in accordance with our first critical remark, the curves are truncated at 70Hz.

DISCUSSION

The weakest aspect of the $V_{P_{\text{cal}}}(f)$ curves as calculated in this approach is the absolute scale. The calibration, matching the high frequency phase velocity to the time domain velocity pick, arguably has removed the worst of the bias, but it is difficult to be completely certain of the numbers on the vertical axis of Figure 10. The strongest aspect is the character and curvature of the $V_{P_{\text{cal}}}(f)$ estimates, i.e., the relative values of $V_{P_{\text{cal}}}$ at one versus another frequency. The curvature in the lower half of the frequency band is a direct result of the curvature in the Gabor spectra of the arrivals (see Figure 7). This effect is visible to the eye, and is unlikely to be an artifact.

The significance of the variability of one $V_{P_{\text{cal}}}(f)$ curve from another (i.e., the separation of the dashed lines in Figure 10b) depends on the perceived level of heterogeneity in the geology in the upper 150m spanned by the wave paths used in this study. If the medium is fairly homogeneous in its dispersive properties, which is supported by the independent work of Montano et al. (2015), then the single standard deviation in Figure10b indicates the certainty and repeatability of the $V_{P_{\text{cal}}}(f)$ estimation. The expansion of the error at higher frequencies is an indication of the increasing sensitivity of the calculation to uncertainty in inputs which appear in the denominator of the calculation. However, if we are less certain of the homogeneity of the dispersive properties of the medium, the spread of estimates

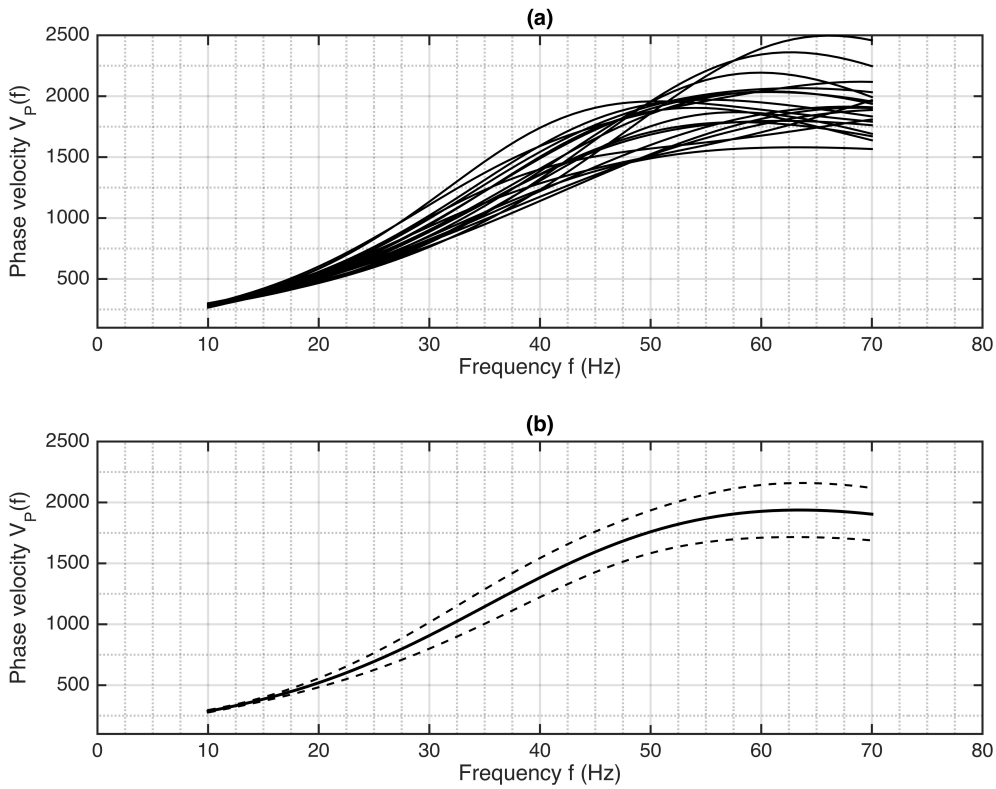

FIG. 10. (a) Phase velocity curves calibrated using the space-time and spectral analysis results illustrated in Figures 2 and 3. (b) Mean (solid line) and $\pm$ one standard deviation (dashed line).

may legitimately reflect spatial variations in $V_{P_{\text{cal}}}(f)$. Because the VSP experiment begins at a depth of 76m, the region above this point is poorly constrained, and justification for assuming homogeneity in the very near surface is difficult to produce. Therefore, we are forced to allow that both methodological uncertainty and near surface heterogeneity both contribute to the separation of the dashed lines in Figure 10b.

The most frequently used models for attenuation and dispersion assign to the medium a parameterized dispersion rule. For instance, neglecting attenuation in the nearly constant Q model discussed by Aki and Richards (2002), the phase velocity has the assumed form:

$$V_P(\omega) = V_{P_0}\left[1 + \frac{1}{\pi Q}\log\left(\frac{\omega}{\omega_0}\right)\right]. \tag{11}$$

In Figure 10 the dispersion has been calculated in an unconstrained manner, i.e., frequency by frequency from the data. No "rule" involving, for instance, $\log\omega/\omega_0$ has been imposed on the estimation. Considerations of causality require that the dispersion be part of a legitimate attenuation-dispersion pair, in accordance with the Kramers-Krönig relations, but the existence, or not, of a match between Figure 10 and equation (11) must be ascertained. However, the negative curvature of the average estimated $V_{P_{\text{cal}}}(f)$ at the lower frequencies and the order of magnitude variation in phase velocities between 10-20Hz and 70-80Hz make it difficult to fit it to a standard model such as the one in equation (1).

Are these features of $V_{P_{\text{cal}}}(f)$ real? There seems to be reason to at least provisionally accept them. The low-frequency curvature in Figure 10 is certainly present in the data, and is correlated with the positive curvature at low frequency in the arrival time picks in Figure 7. Thus, to criticize this part of the derived $V_{P_{\text{cal}}}(f)$ we must ascribe the curvature in Figure 7 to other effects. Near field coupling is a source of apparent dispersion, however, even at 10Hz, the geophone, which is between 300-400m away from the source, is outside of the wavelength by a factor of at least 3-4$\times$. The absolute velocity numbers after calibration vary strongly, but they are not unrealistic: for instance, uphole land surveys have reported variations in P-wave velocity from 500m/s in the upper 10s of metres to 2000m/s in the 100-200m regime (Guevara et al., 2013). Finally, the results in Figure 10 are quite stable across 20 independent estimates, especially at low frequency.

Thought experiment: vibroseis sweep and dispersion as counteracting phenomena

The two processes "vibroseis sweep" and "body wave dispersion" counteract one another in their influence on the geophone response. The sweep progressively delays the arrival at a geophone of high frequencies, and dispersion progressively speeds them up. Thus it is true that in the presence of dispersion, there will exist certain pairs of nearby frequencies which departed the source at different times but arrive at a geophone simultaneously. Because correlation answers the question: "what would the geophone response have been if all frequencies had arrived simultaneously?", it is correct to say that a dispersive geological volume is a partial correlator of vibroseis signals. The degree of meaningful correlation in practice is so small as to make this a theoretical point of interest only. However, it is interesting to recognize that, for any given source and geophone pair embedded in any given dispersive geological volume, there exists one unique vibroseis sweep program for which all frequencies arrive at the geophone simultaneously. Put another way,

for every source/receiver pair in every dispersive volume there is one unique sweep which self-correlates.

CONCLUSIONS

Uncorrelated vibroseis data provide a means, as has been pointed out by several researchers, to characterize seismic body wave dispersion. Based on concerns that a poorly characterized and/or poorly parameterized dispersion model, coupled with low Q, in the near surface and/or ocean bottom will expose FWI to unrecoverable uncertainty, we examine raw vibroseis data for its ability to provide unconstrained estimates of $V_P(f)$ in a near surface environment. Average phase velocities along (assumed) straight ray paths are determined by picking first arrivals from Gabor spectra of traces from a walkaway VSP data set. Phase velocities ranging from roughly 500m/s to 2000m/s over the 10-70Hz band are determined, with a roughly sigmoidal curvature. These results are interesting in that they do not support the use of a standard nearly constant Q model, whose low-frequency curvature is positive rather than negative. Recommendation is to seek confirmation with further field testing of the methodology, possibly using different time-frequency decomposition tools. Demonstrating an independence of the derived $V_P(f)$ curve from a particular processing method would provide additional confirmation that the variation is meaningful.

ACKNOWLEDGEMENTS

We thank the sponsors of CREWES for continued support. This work was funded by CREWES and NSERC (Natural Science and Engineering Research Council of Canada) through the grant CRDPJ 461179-13. Kevin Hall and Malcolm Bertram are thanked for technical suggestions. An unidentified company is acknowledged for access to the dataset.

REFERENCES

Aki, K., and Richards, P. G., 2002, Quantitative Seismology: University Science Books, 2nd edn.

Dragoset, W., 1988, Marine vibrators and the Doppler effect: SEG Expanded Abstracts, 75–78.

Futterman, W. I., 1962, Dispersive body waves: Journal of Geophysical Research, **67**, 5279–5291.

Guevara, S., Margrave, G. F., and Agudelo, W. M., 2013, Near-surface S-wave velocity from an uphole survey using explosive sources: CSEG Geonconvention Expanded Abstracts.

Haase, A. B., 2010, q estimation from uncorrelated vibroseis vsp model data: CSEG Geonconvention Expanded Abstracts.

Hak, B., and Mulder, W. A., 2010a, Migration for velocity and attenuation perturbations: Geophysical Prospecting, **58**, 1–13.

Hak, B., and Mulder, W. A., 2010b, Seismic attenuation imaging with causality: Geophysical Journal International, **184**, No. 1, 439–451.

Hall, K. W., Lawton, D. C., Holloway, D. E., and Gallant, E. V., 2012, Husky 2011 Walkaway 3C-VSP: CREWES Annual Report.

Hargreaves, N. D., and Calvert, A. J., 1991, Inverse Q-filtering by Fourier transform: Geophysics, **56**, 519–527.

Hicks, G., and Pratt, R. G., 2001, Reflection waveform inversion using local descent methods: estimating attenuation and velocity over a gas-sand deposit: Geophysics, **66**, 598–612.

Innanen, K. A., and Lira, J. E., 2010, Direct nonlinear Q compensation of seismic primaries reflecting from a stratified, two-parameter absorptive medium: Geophysics, **75**, No. 2, V13–V23.

Innanen, K. A., and Weglein, A. B., 2007, On the construction of an absorptive-dispersive medium model via direct linear inversion of reflected seismic primaries: Inverse Problems, **23**, 2289–2310.

Kamei, R., and Pratt, G., 2013, Inversion strategies for visco-acoustic waveform inversion: Geophysical Journal International, **194**, No. 2, 859–884.

Kjartansson, E., 1979, Constant-Q wave propagation and attenuation: Journal of Geophysical Research, **84**, 4737–4748.

Margrave, G. F., 2015, Stratigraphic filter and Q estimation: CSEG Expanded Abstracts.

Métivier, L., Brossier, R., Operto, S., and Virieux, J., 2015, Acoustic multi-parameter FWI for the reconstruction of P-wave velocity, density and attenuation: preconditioned truncated Newton approach: SEG Expanded Abstracts, 1198–1203.

Montano, M. C., Lawton, D. C., and Margrave, G. F., 2015, Shallow q_p and q_s estimation from multicomponent VSP data: CSEG Geoconvention Expanded Abstracts.

Moradi, S., and Innanen, K. A., 2015, Scattering of homogeneous and inhomogeneous seismic waves in low-loss viscoelastic media: Geophysical Journal International, **202**, 1722–1732.

Ribodetti, A., and Virieux, J., 1998, Asymptotic theory for imaging the attenuation factor Q: Geophysics, **63**, 1767–1778.

Sun, L. F., and Milkereit, B., 2007, Velocity dispersion and attenuation in vibroseis data: CSEG Geonconvention Expanded Abstracts.

Sun, L. F., Milkereit, B., and D.Schmitt, 2009, Measuring velocity dispersion and attenuation in the exploration seismic frequency band: Geophysics, **74**, No. 2, WA113–WA122.

Tonn, R., 1991, The determination of the seismic quality factor Q from VSP data: a comparison of different computational methods: Geophysical Prospecting, **39**, 1–27.

Zhang, C., and Ulrych, T. J., 2007, Seismic absorption compensation: a least squares inverse scheme: Geophysics, **72**, R109–R114.